J. Phys.: Condens. Matter **20** (2008) 474210 (8pp) doi:10.1088/0953-8984/20/47/474210

Fabrication of superconducting MgB_2 nanostructures

C Portesi[1], E Monticone[1], S Borini[1], G B Picotto[1], N Pugno[2,3] and A Carpinteri[1,2]

[1] INRIM—Istituto Nazionale di Ricerca Metrologica, Strada delle Cacce 91, I-10135 Torino, Italy
[2] Department of Structural Engineering, Politecnico di Torino, Corso Duca degli Abruzzi 24, 10129, Torino, Italy
[3] National Institute of Nuclear Physics, National Laboratories of Frascati, Via E Fermi 40, 00044, Frascati, Italy

E-mail: c.portesi@inrim.it

Received 21 April 2008, in final form 17 October 2008
Published 6 November 2008
Online at stacks.iop.org/JPhysCM/20/474210

Abstract
Electron beam lithography has been used for the fabrication of superconducting magnesium diboride nanofilms (thickness lower than 100 nm), which were then characterized by atomic force microscopy. The analysis reported in this paper demonstrates that these nanofilms have self-affine surfaces with a fractal dimension of ∼2.25. A size-effect on the critical temperature for activating the superconductive state is discussed and fractal scaling laws are consequently proposed. Only a moderate reduction of the critical temperature is imposed by the shrinking of the investigated nanofilms with respect to their bulk counterpart, suggesting that MgB_2 nanostructures could play a fundamental role in superconductive nanocircuits.

1. Introduction

In the last few years, great efforts have been devoted to the fabrication of MgB_2 nanobridges, which could play a crucial role in the field of applied superconductivity. In fact they can act as weak-links in superconducting devices, e.g. SQUIDs [1–4] or superconducting nanotransistors (SNTs) [5]. Possible applications of MgB_2 nanostructures in superconducting single-photon detectors (SNTDs) could also be investigated. There are several reasons for the great interest in possible applications of magnesium diboride nanostructures. First, the discovery of superconductivity at 39 K in MgB_2 (January 2001 [6]) opened new perspectives in the superconductivity field thanks to the interesting properties of this material (relatively high T_c, energy gap similar to that of NbN, moderate anisotropy, transparency of the grain boundaries). Moreover, replacing the traditional Josephson junction (JJ)-based devices with superconducting weak-links could have some advantages, considering that current JJ devices have limited applications (partially due to their difficult fabrication). Superconducting single-photon detectors (SSPDs) in recent years have been the subject of growing technological interest: they are already used as diagnostic tools for integrated circuits on a large scale, but their most promising applications are in space optical communications and quantum cryptography. The interest in fabricating this type of device on MgB_2 film resides in the following considerations. First, an MgB_2-based detector would work at temperatures of 15–20 K (instead of 4.2 K required for NbN detectors), without any significant drawback in terms of detecting rate, detectable spectrum range and other properties. This is due to the fact that MgB_2 has a critical temperature of 39 K, but two energy gaps (Δ_σ and Δ_π), the smallest of which (Δ_π, dominant in all isotropic processes) is about 3 meV wide (for NbN, $\Delta =$ 2 meV). Additionally, the high operating temperature of MgB_2 detectors would allow for using compact and cheap cooling systems (e.g. single-stage cryocoolers), with great advantage for satellite applications. Moreover, at higher temperature the thermal impedance at the film/substrate interface is expected to be lower, leading to a faster response time for the detector.

In the literature, different methods for fabrication of MgB_2 nanobridges have been exploited. Beside the well-known focused ion beam (FIB) technology, electron beam lithography (EBL) methods have been experimented too, with encouraging results [5, 7]. In our previous work [5], it has been demonstrated that the EBL nanostructuring process does not affect the electrical properties of the starting material, so that

superconducting MgB_2 nanowires can be obtained with widths down to 180 nm.

In this paper, part of the work has been devoted to the study of the film surface by atomic force microscopy (AFM) and the AFM data have been analysed by a dimensional method, based on the scaling of a surface property with the measurement area size. As commonly used for fractal analysis, the surface line profiles have been studied. This type of surface analysis has been carried out since, as is well known, for the fabrication of superconducting devices based on superconducting nanostructures where the quality of the starting surface is often of crucial importance to the optimal operation of the device. For example, the transport properties of superconducting nanobridges are strongly affected by the geometry and the edge definition of the nanostructures itself.

Then, we refer to the fabrication and the characterization of MgB_2 nanostructures fabricated by an EBL-based approach and our attention is mainly devoted to samples with thickness lower than 100 nm. Electrical and superconducting properties of nano-and microstructured samples have been compared to those of the unstructured film.

This work demonstrates the possibility of fabricating superconducting MgB_2 nanostructures based on magnesium diboride films fabricated by an all-*in situ* method and thinner than 100 nm. The main advantages of our method are the following. First, by the all-*in situ* method, no poisoning gases are involved and relatively low temperature are reached. Moreover, if compared to other nanostructuring techniques, (e.g. FIB), EBL is more flexible and excludes any risk of ion implantation.

These results constitute a step toward the fabrication of MgB_2-based devices such as SSPDs.

2. Experimental details

MgB_2 films were deposited on Si/SiN(500 nm) and sapphire substrates by the all-*in situ* method [8], based on the co-evaporation of B and Mg by means of an e-gun and a resistive heater, respectively. During the deposition, the substrate temperature was held at a constant value of 295 °C and the evaporation rate was fixed at a nominal value of 1 Å s^{-1} for B and twice as high for Mg. The MgB_2 precursor was then annealed in the deposition chamber at 500 °C for 5 min.

2.1. AFM equipment

Quantitative measurements of topography parameters and critical dimensions of these structures have been carried out by means of a metrological scanning probe microscope (SPM) [9]. Precise surface topography reconstruction by SPM, optical and stylus profilometry needs instruments with accurate, stable and traceable devices able to minimize and/or control nonlinear motions, pitch, roll and yaw, hysteresis and drifts of the relative tip/sample movements when scanning the surface to be imaged. Moreover, small mechanical measurement loops between tip and sample and a good matching of the used materials are needed to minimize drifts. Other significant errors in the surface profile reconstruction are due to the probe–sample interactions and finite size/geometry of the tip, namely when imaging small and high-aspect ratio surface structures. These errors can be partly corrected afterwards by image analysis, on the assumption of a good repeatability of scanners. Metrological SPM instruments make use of active controls of tip/sample displacements measured by traceable position monitors, e.g. laser interferometers or capacitive sensors, to be used with the position monitors at negligible Abbé offsets [10]. The use of laser interferometers provides direct traceability to the wavelength of light, at the cost of a more complex setup of the compact scanning systems. Our SPM makes use of a sample-moving scanning device working up to tens of micrometres and driven by interferometers for the xy axis and capacitive sensors integrated in a tripod-type assembly for the z-axes. The home-made SPM system uses the software and electronic control of a commercial AFM platform from APE Research Srl. The imaging of these structures has been performed by contact AFM with ultra sharp AFM tips.

2.2. Fabrication of nanostructured samples

The structuring process for fabricating samples with nanometric features consisted of the following steps. First, a Ti film about 50 nm thick was deposited on magnesium diboride films by e-beam evaporation. Then, the e-beam resist (PMMA) was spin coated on the samples at 4000 rpm for 45 s and baked at 165 °C for 5 min. The desired nanopatterns were e-beam written and developed selectively in PMMA developer (MIBK:IPA 1:3 in volume). Then, the uncovered Ti was removed by reactive ion etching (RIE) in CF_4, and the PMMA was dissolved in acetone. Hence, the removal of magnesium diboride was carried out by physical milling (Ar milling), using the Ti film as a mask layer and taking advantage of its lower etching rate compared to that of MgB_2 under Ar ion bombardment. The last steps consisted of optical lithography and physical etching of a MgB_2/Ti bilayer for defining the microcircuit and hence measuring the electrical properties of the nanostructures.

The EBL process was carried out in a Jeol840 scanning electron microscope (SEM) equipped with a NanoPattern Generator System (NPGS) by JC Nabity, employing an accelerating voltage of 35 kV and a beam current of 30 pA. The electron dose was fixed at 340 μC cm^{-2}. In these conditions, we were able to control the fabrication of nanostructures. The single-layer PMMA electron resist, used as a mask for the RIE process for forming the nanowires on Ti films, was about 200 nm thick and it ensured a reliable protection of the superconducting film.

The physical etching of Ti was carried out in a RIE system, using a CF_4 pressure of 0.5 mbar, flux of 180 sccm and input power of 100 W, which leads to an etching rate of about 4 nm s^{-1}.

The physical removal of MgB_2 was performed by an ECR plasma system operating at 2.45 GHz. It was carried out at Ar pressure of 1.0×10^{-3} mbar and, using an extraction voltage of 400 V and an anode current density of 1.5 mA cm^{-2}, an etching rate of 2 Å s^{-1} has been obtained.

During the Ar milling the resist layer was thinned and it was then completely removed in acetone.

The nanostructures have been imaged by SEM and AFM and their electrical and transport properties have

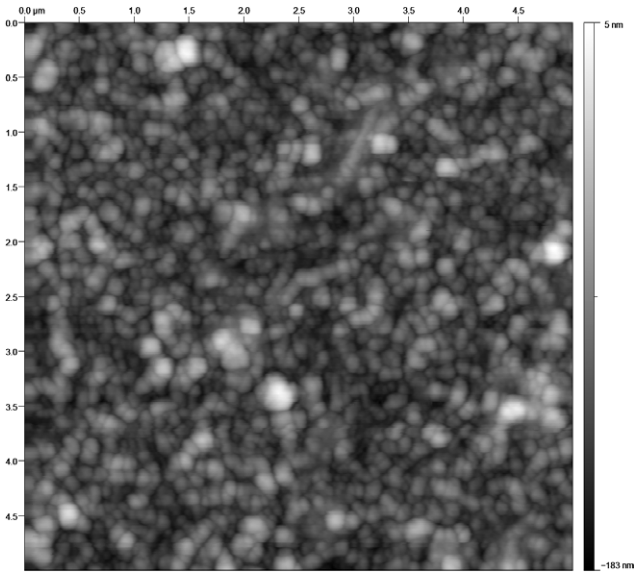

Figure 1. AFM image with area of 5 μm × 5 μm of an MgB_2 film. The film is grown by the all-*in situ* method.

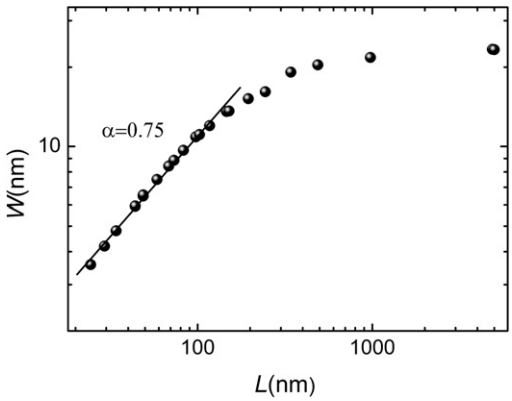

Figure 2. $w(L)$ as a function of L calculated on the AFM image (with area of 5 μm × 5 μm) reported in figure 1. At low w the typical L^α dependence is observed, with a value of α of 0.75 (fractal dimension $D = 2.25$).

been evaluated by four-wire measurement in a single-stage cryocooler with a base temperature of 9 K and stability of ±0.01 K.

3. Results and discussion

The AFM image with area 5 μm × 5 μm of an MgB_2 film is reported in figure 1. The sample has a mounded surface constituted of rounded grains grown on columnar pillars.

Among many approaches to measuring the fractal dimension, we used a dimensional method based on the analysis of surface line profiles: it is commonly employed for fractal analysis, since the intersection of a self-affine fractal surface by a vertical plane yields a profile or trace that is also self-affine with fractal dimension smaller by about one than that corresponding to the surface [11, 12]. The most used method consists in obtaining the so-called 'interface width' defined for a sample of lateral dimension L [13] or the scale dependent surface roughness, $w(L)$, defined as the variance of the height, h, over a profile of length L, i.e.

$$w(L) = \sqrt{\frac{1}{N_L}\sum_{J=1}^{N_L}[h_j - \overline{h(L)}]^2} \qquad (1)$$

where N_L is the number of points in the profile of length L, h_j is the height at point j and $\overline{h(L)}$ is the average height in the profile of length L. In the case of film growth, because of the dependence of h on time, the interface width is sometimes written as $w(L,t)$ and h_j as $h_j(t)$. For a self-affine surface, $w(L)$ scales as L^α for $L \ll \xi$ where ξ is the lateral correlation length and $w(L,t) \sim t^\beta$ for $L \gg \xi$ where β is the dynamic exponent. In the case of roughness, the L^α dependence yields to α, the roughness exponent. This parameter is related to the fractal dimension by $D = d + 1 - \alpha$, with d the dimension of the interface (2 for surfaces). The saturation value of w yields to the total width of the interface, that is $R_q = w(L_f)$, L_f being the linear size of the measured frame. R_q is related to the root mean square (rms) roughness.

In figure 2 the results of the analysis are shown. The curve reported here refers to an AFM image with area of 5 μm × 5 μm. For low L the typical L^α dependence is observed. On the other hand, at high L the saturation of w takes place, yielding the total width of the interface. In this case, α has a value of 0.75. α can range between 0 and 1, for self-affine fractal surfaces: usually, a large value of $\alpha(>0.5)$ corresponds to a smooth textured surface structure in a short range while a smaller value of $\alpha(<0.5)$ corresponds to a more jagged local surface morphology [14].

A roughness exponent between 0.65 and 1 is typically observed on metal thin films where surface diffusion plays a dominant role. An important class of growth models with the previous characteristics is accounted for in the Villain, Lai and Das Sarma (VLDS) theory [15] where $\alpha = 0.66$ and $\beta = 0.2$ for growth in two-dimensional substrates.

As estimate of β is not easily feasible, thus an alternative method using the analysis of roughness distribution is introduced [16]. The roughness distributions is given by,

$$P(w) = \frac{1}{\sigma}\psi\left(\frac{w - \langle w\rangle}{\sigma}\right) \qquad (2)$$

where $P_L(w)\,\mathrm{d}w$ is the probability that width w of a given configuration lies in the range $[w, w + \mathrm{d}w]$ and $\sigma \equiv (\langle w^2\rangle - \langle w\rangle^2)^{1/2}$ is the rms deviation of w.

The roughness distributions $P(w)\sigma$ of the film surface in figure 1 is shown in figure 3.

Previous studies [17] suggest for the two-dimensional VLDS class a simple exponential decay of the $P(w)$ tail. By fitting the data in figure 3 with $\exp(-bx^\gamma)$ between 0 and 4 we find $\gamma = 1.2 \pm 0.07$ that is slightly higher than the expected value for the VLDS class. Thus, we expect that the film roughness increases with the thickness t according to a power law t^β with $\beta = 0.2$.

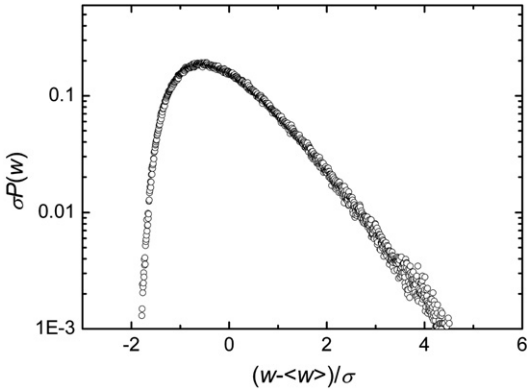

Figure 3. The normalized roughness distributions $\sigma P(w)$ of the film surface in figure 1.

3.1. Characterization of MgB_2 nanostructures

At first, for fabrication of nanostructures we used MgB_2 films with thickness ranging from 100 to 150 nm. The choice of working on film with this thickness was a compromise between two aspects: on one hand, the higher the thickness of the film, the better are the electrical and transport properties. On the other hand, working on samples thicker than 150 nm could prevent the fabrication of good quality and narrow nanostructures.

The correlation between the electrical properties and the film thickness is confirmed by data plotted in figures 4(a) and (b), where the critical temperature T_c and the $1/RRR$ (RRR = residual resistivity ratio) are reported as a function of the thickness and of 1/thickness respectively, for a set of films either on silicon nitride (open circles) or sapphire (squares) substrates. In figure 4(b), we plotted the inverse of the residual resistivity ratio ($1/R = R(40\ \mathrm{K})/R(300\ \mathrm{K})$) instead of the resistivity itself in order to obtain any possible error due to the geometry of the sample.

The results obtained in the fabrication of the first MgB_2 nanostructures 100–150 nm thick have been reported and discussed elsewhere [5, 18, 19]. Summarizing, the critical temperature and the transition width of nanobridges were not dramatically changed because of the structuring process. Their critical current density was calculated to be of the order of 1×10^6 A cm^{-2} at 10 K, which is a considerable value, taking into account that the nanobridges fabricated by FIB on the best MgB_2 thin films [20] showed a J_c of 5×10^7 A cm^{-2} at 4.2 K and an increase of J_c by a factor of 2 is expected for our films going from 10 K down to 4.2 K.

Next, we investigated the properties of nanostructures (bridges and meanders) based on magnesium diboride films with thicknesses lower than 100 nm. This has been done since the final purpose of our work is the fabrication of superconducting devices, such as SSPDs, which usually requires very low thickness for obtaining good performances.

As a preliminary investigation, we studied the electrical properties (resistivity, transition temperature and width etc) of a microstrip, a nanobridge 600 nm wide and a meander line 370 nm wide (the three of them all based on the same MgB_2 sample 80 nm thick) and we compared the results to those of the unstructured film. For the fabrication of samples with comparable characteristics, we proceeded as follows: the film was deposited by the all-*in situ* method described above, then the electrical properties of the unstructured sample were characterized by four-wire measurement. Before the structuring of the film, the substrate was cut in two pieces, one for the nanobridge and one for the meander. Then, the two samples were structured by an EBL-based process and optical lithography (see section 2) for obtaining the measurable micrometric circuit containing the nanostructure.

In figure 5, the SEM images of the nanostructures are reported. The nanobridge (figure 5(a)) is 1 μm long and 650 nm wide; the seven nanofeatures of the meander line are 360 nm wide and 3 μm long each. In the inset of figure 5(b) the image of the whole structure is reported. The micrometric strips including the nanostructures had a width of 10 μm.

The electrical and superconducting properties of both the nanobridge and the meander have been evaluated and compared to those of the microstrip 10 μm wide.

From the electrical characterization at low temperature, the calculation of the resistivities for strip, nanobridge and meander has been performed, taking into account the geometry of the sample. The values that have been obtained are 172 $\mu\Omega$ cm, 371 $\mu\Omega$ cm and 572 $\mu\Omega$ cm respectively. These resistivity values are in agreement with values reported in our previous works [18, 19] and referred to MgB_2 microstrip and

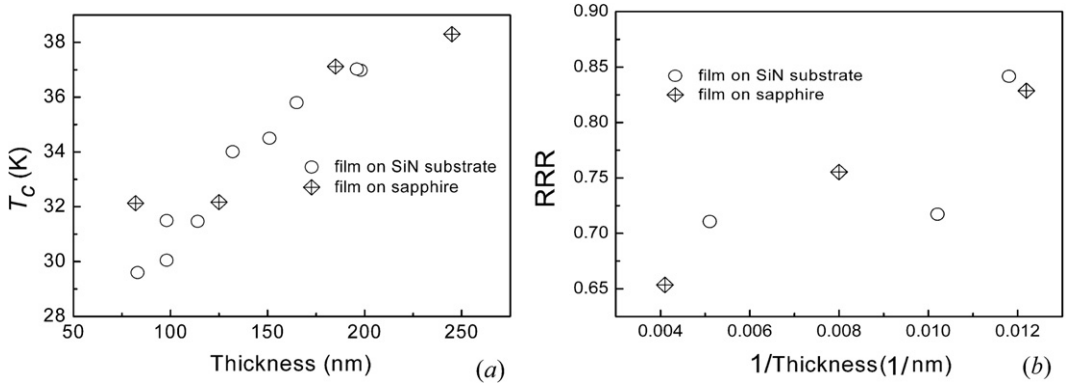

Figure 4. Critical temperature and *RRR* are plotted as a function of thickness (a) and 1/thickness (b), respectively. Open circles refer to film deposited on silicon nitride substrates and cross-squares refer to film on sapphire.

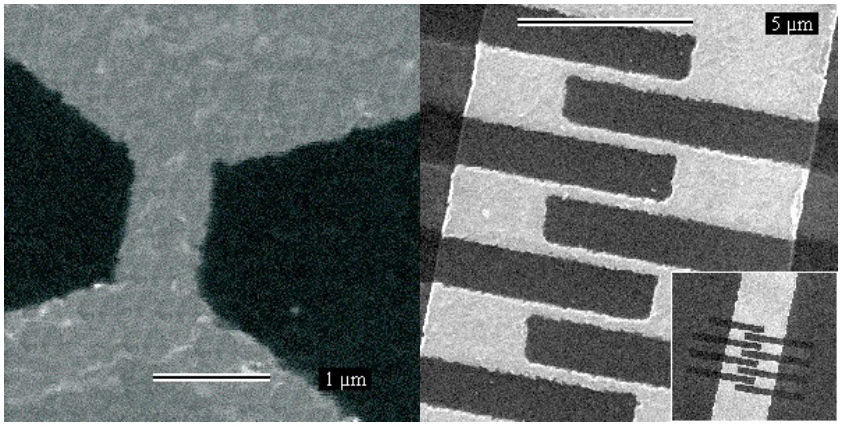

Figure 5. SEM images of the nanobridge (a) and of the meander (b) based on an MgB_2 film 80 nm thick. The bridge is 1 μm long and 650 nm wide. The nanostrips constituting the meander are 360 nm wide and 3 μm long. In both case, the two nanostructures are included in a microstrip 10 μm wide.

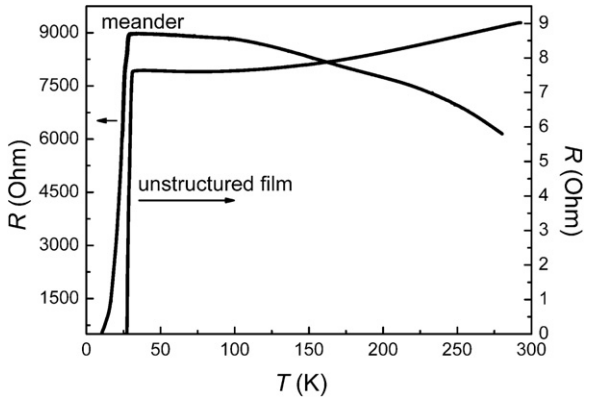

Figure 6. $R(T)$ measurements from room temperature down to 10 K for the unstructured MgB_2 film and the strip featuring the meander line 360 nm wide.

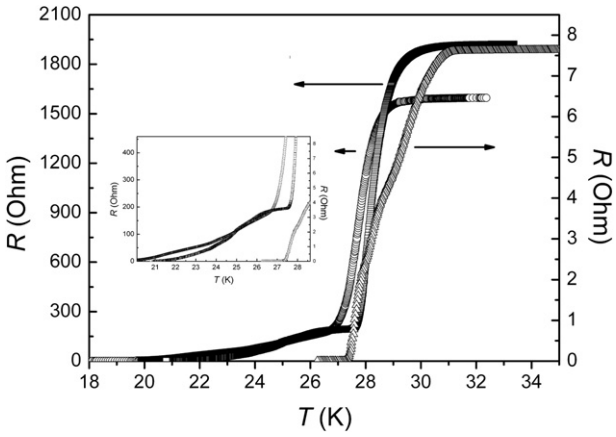

Figure 7. $R(T)$ curves of the unstructured sample (△), of the micrometric strip (○) and the nanobridge (□). In the inset the details of the last part of the transition (where a bumped profile is observed) are reported.

nanobridges. According to Rowell [21], our MgB_2 films can be classified as magnesium diboride samples with intermediate resistivity and it has been pointed out that the resistivity values in this intermediate regime can be explained by arguments involving both high residual resistivities and reduced effective areas [21].

By comparing the $R(T)$ curves of the unstructured film and of the meander from room temperature down to 10 K (figure 6), it is clear that the structured sample has a non-metallic behaviour that may be indicative of intergrain quasiparticle tunnelling, which becomes evident in the presence of nanoconstrictions limiting the percolation path for the electrical current [22].

On the other hand, in the case of the meander, even at 10 K we have a residual resistance of 500 Ω in the $R(T)$ curve, probably due to a damaged nanostrip of the meander line. Even if it is noteworthy that the T_{conset} (where T_{conset} is the temperature at which the resistance starts to drop) is 28.6 K both for meander and unstructured film, nevertheless any further consideration can still be done. Therefore, in the following discussion we will not consider anymore the $R(T)$ measurement of the meander.

In figure 7 the $R(T)$ curves of the unstructured film, of the micrometric strip and of the nanobridge are reported.

According to results reported in our previous work, the nanostructuring process does not affect the superconducting properties of magnesium diboride. All three curves show a splitting of the resistive transition on two features, which become more evident as a consequence of the nanostructuration (as emphasized in the inset of figure 7). We observed the splitting of the resistive transition in several MgB_2 films grown by all-*in situ* methods. We have not yet performed a systematic study of this behaviour in the $R(T)$ curves, nevertheless, we observe that a splitting of the resistive transition in magnesium diboride has been measured and studied by others [23] as well. In [23], the authors assume that the conductivity of a multiphase superconductor near the transition behaves as a parallel association of

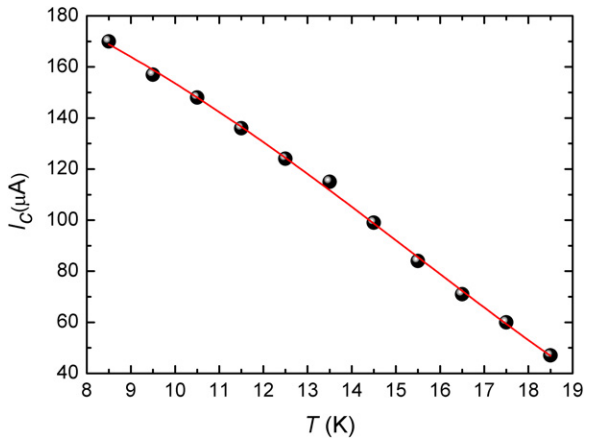

Figure 8. Critical current of the MgB_2 nanobridge plotted as a function of temperature. Experimental data are fitted by $I_c = I_{c0} \cdot (1 - T/T_c)^{\gamma} \cdot (1 - T/T_c)^{1/2}$, where $\gamma = 3 - T/T_c$. (This figure is in colour only in the electronic version)

contributions and consider that the split of resistive transition in MgB_2 may be due to nonpercolating regions of the sample submitted to tensile strains that locally change T_c. Analogous splittings of the resistive transition have also been observed in several samples of high T_c cuprate superconductors (systems structurally and electronically much more complex than MgB_2) [24, 25]. The observed split resistive transition in this case might have similar origin to that observed in MgB_2. Of course, further investigations are needed to understand this phenomenon.

Furthermore, the nanobridge shows a critical temperature slightly higher than the microstrip, but this is probably due to small inhomogeneities of the starting unstructured film. In the $R(T)$ curve of the nanobridge, the splitting of the resistive transition is clearly revealed by the knee at about 192 ohm. Therefore, we identify two characteristic temperatures T_c^1 (at 28.3 K) and T_c^2 (at 24.7 K), which are interpreted as representative of critical superconducting temperatures. Hence, we are led to assume that two different superconducting phases are still present in our structured samples (at zero magnetic field). Moreover, the nanobridge transition width is comparable to that of the microstrip and the unstructured film, while for uniform superconducting nanostructures a narrower transition would be expected. In this case the form of the $R(T)$ dependency is mainly determined by particular distribution of imperfections within the sample.

The critical current of the nanobridge has also been measured at different temperatures ranging from 8.5 K (lowest temperature reachable by the cryocooler employed) to 18.5 K. The results are shown in figure 8. According to [1], the critical current is expected to be proportional to λ^{-2} and ξ^{-1}. Given the temperature dependencies of λ and ξ, $\lambda = \lambda_0/((1 - T/T_c)^{\gamma})^{1/2}$ [26] and $\xi = \xi_0(1 - T/T_c)^{-1/2}$, the critical current is expected to behave as $I_c = I_{c0} \cdot (1 - T/T_c)^{\gamma} \cdot (1 - T/T_c)^{1/2}$, where $\gamma = 3 - T/T_c$.

The calculated critical current density J_{c0} is about 5×10^5 A cm^{-2}. This value, even if still consistent with values in the literature for MgB_2 thin film [27, 28], is lower than that calculated for our thicker films [5, 18, 19]. On the other hand, the higher sensitivity of thinner films to deterioration during patterning has also been observed in the literature for different superconducting materials [29, 30]. Actually, during patterning any damage at the surface affecting the topmost layers of the film will have a much larger effect on the properties of a thinner film than of a thicker one. This issue could probably be overcome by depositing an Au protecting layer on the as-grown films.

The analysis of the electrical characterization of the structured samples and as-grown films with thickness lower than 100 nm confirms that the EBL-based technique is suitable for fabrication of MgB_2 nanostructures without detrimental effect on the superconducting properties of the film. Since the main purpose of our work in this field is the fabrication of superconducting devices (e.g. SSPDs), our efforts have been devoted to the fabrication of magnesium diboride nanostructures on sapphire. In fact, for fabricating SSPDs, sapphire is a more suitable substrate, thanks to its characteristics, such as good thermal conductance, optical transparency combined with good structural and morphological properties for growing MgB_2 films. The preliminary results in this direction have been presented elsewhere [31]. In summary, MgB_2 bridges from 600 nm to 800 nm wide and 40 nm thick have been obtained. The T_c in this case was rather low (about 25 K) due to the film thickness, and the calculated resistivity was about 250 $\mu\Omega$ cm.

4. Scaling law of the critical temperature

The critical temperature reduction could be in part due to small grain dimensions. Making an analogy between the electrical and mechanical resistances, the critical temperature in superconductivity plays the role of the energy release rate in brittle fracture. We thus expect a scaling of the critical temperature as a function of the fractal exponent in the form of [32]:

$$T_c \propto L^{\frac{3-D}{2}}. \tag{3a}$$

In addition, including the moderate variability of the fractal exponent by increasing the size-scale (from 2 to 3) one would expect the following scaling [27]:

$$T_c = T_c^{(\mathrm{macro})} \left(1 + \frac{\ell}{L}\right)^{-1/2} \tag{3b}$$

where ℓ is a characteristic internal material length (e.g. grain size) and L the film thickness. Moreover, considering a cut-off for nanoscale applications would imply:

$$T_c = T_c^{(\mathrm{macro})} \left(1 + \frac{\ell}{L + \varepsilon}\right)^{-1/2} \tag{3c}$$

where the length ε defines the critical temperature at the nanoscale via $T_c^{(\mathrm{nano})} \equiv T_c^{(\mathrm{macro})}(1 + \frac{\ell}{\varepsilon})^{-1/2}$. We thus propose the use of the phenomenological equation (3*c*) in order to design superconductive nanofilms. For example for MgB_2 structures we have measured $T_c^{(\mathrm{nano})} \approx$ 25–28 K, $T_c^{(\mathrm{macro})} \approx$ 32–38 K and $\ell \approx w \approx$ 1–10 nm.

5. Conclusion

The AFM study of magnesium diboride thin film surfaces demonstrates that these films have self-affine surface structure with smooth textured structure in a short range. We calculated a value for α of 0.75. This parameter can range between 0 and 1, for a self-affine fractal surface: usually, a large value of α (>0.5) corresponds to a smooth textured surface structure in a short range while a smaller value of α (<0.5) corresponds to a more jagged local surface morphology [14].

The results of the electrical characterization of the nanostructures show that the EBL-based method for structuring magnesium diboride films is suitable for fabricating MgB_2 nanobridges and meanders. Since the studied samples have a thickness lower than 100 nm, their T_c is not as high as for the best samples fabricated by the *in situ* method (32–38 K). On the other hand, in perspective of electronic applications, the critical temperature of the nanostructures can be considered not as crucial as their thickness, which must be small enough in order to guarantee fast and homogeneous thermalization. Therefore, these preliminary results can be considered as a successful step towards the fabrication of new superconducting single-photon detectors. In the near future, our efforts will be devoted to the fabrication of MgB_2 nanostructures, on silicon nitride and sapphire substrate, with a width of the order of 100–200 nm.

References

[1] Brinkman A, Veldhuis D, Mijatovic D, Rijnders G, Blank D H A, Hilgenkamp H and Rogalla H 2001 Superconducting quantum interference device based on MgB_2 nanobridges *Appl. Phys. Lett.* **79** 2420–2

[2] Mijatovic D, Brinkman A, Veldhuis D, Hilgenkamp H, Rogalla H, Rijnders G, Blank D H A, Pogrebnyakov A V, Redwing J M, Xu S Y, Li Q and Xi X X 2005 SQUID magnetometer operating at 37 K based on nanobridges in epitaxial MgB_2 thin films *Appl. Phys. Lett.* **87** 192505

[3] Portesi C, Mijatovic D, Veldhuis D, Brinkman A, Monticone E and Gonnelli R S 2005 MgB_2 magnetometer with a directly couplet pick-up loop *Supercond. Sci. Technol.* **19** 303–6

[4] Burnell G, Kang D J, Ansell D A, Lee H N, Moon S H, Tarte E J and Blamire M G 2002 Directly coupled superconducting quantum interference device magnetometer fabricated in magnesium diboride by focused ion beam *Appl. Phys. Lett.* **81** 102–4

[5] Portesi C, Borini S, Monticone E and Amato G 2006 Fabrication of superconducting MgB_2 nanostructures by an electron beam lithography-based technique *J. Appl. Phys.* **99** 066115

[6] Nagamatsu J, Nakagawa N, Muranaka T, Zenitani T and Akimitsu J 2001 Superconductivity at 39 K in MgB_2 *Nature* **410** 63–4

[7] Malisaa A, Charlebois S and Lindström T 2005 Magnesium diboride nanobridges fabricated by electron-beam lithography *J. Appl. Phys.* **98** 124305

[8] Monticone E, Gandini C, Portesi C, Rajteri M, Bodoardo S, Penazzi N, Della Rocca V and Gonnelli R S 2004 MgB_2 thin films on silicon nitride substrates prepared by an *in situ* method *Supercond. Sci. Technol.* **17** 649–52

[9] Picotto G B and Pisani M 2001 A sample scanning system with nanometric accuracy for quantitative SPM measurements *Ultramicroscopy* **86** 247–54

[10] Danzebrink H U, Koenders L, Wilkening G, Yacoot A and Kunzmann H 2006 Advances in scanning force microscopy for dimensional metrology CIRP *Ann. Manuf. Technol.* **55** 841–78

[11] Voss R F 1985 Random fractal forgeries *Fundamental Algorithms for Computer Graphics* ed R A Earnshaw (Berlin: Springer) p 805

[12] Aguilar M, Oliva A I and Anguiano E 1999 The importance of imaging conditions in scanning tunneling microscopy for the determination of the surface texture and roughness *Surf. Sci.* **420** 275–84

[13] Barabasi A L and Stanley H E 1995 *Fractal Concepts in Surface Growth* (New York: Cambridge University Press)

[14] Yang H N, Wang G C and Lu T M 1993 *Diffraction from Rough Surfaces and Dynamic Growth Fronts* (Singapore: World Scientific)

[15] Lai Z W and Das S 1991 Kinetic growth with surface relaxation: continuum versus atomistic models *Phys. Rev.* B **66** 2348–51

[16] Foltin G, Oerding K, Racz Z, Workman L and Zia R K P 1994 Width distribution for random-walk interfaces *Phys. Rev.* E **50** R639–42

[17] Aarao Reis F D 2005 Numerical study of roughness distributions in nonlinear models for interface growth *Phys. Rev.* E **72** 032601

[18] Portesi C, Borini S, Picotto G B and Monticone E 2007 AFM analysis of MgB_2 films and nanostructures *Surf. Sci.* **601** 58–62

[19] Monticone E, Portesi C, Borini S, Taralli E and Rajteri M 2007 Superconducting MgB_2 nanostructures fabricated by electron beam lithography *IEEE Trans. Appl. Supercond.* **17** 222

[20] Zeng X, Pogrebnyakov A V, Kotcharov A, Jones J E, Xi X X, Lysczek E M, Redwing J M, Xu S, Li Q, Lettieri J, Schlom D G, Tian W, Pan X and Liu Z K 2002 *In situ* epitaxial MgB_2 thin films for superconducting electronics *Nat. Mater.* **1** 35–8

[21] Rowell J M 2003 The widely variable resistivity of MgB_2 samples *Supercond. Sci. Technol.* **16** R17–27

[22] Martin S, Fiory A T, Fleming R M, Schneemeyer L F and Waszczak J V 1988 Temperature dependence of the resistivity tensor in superconducting $Bi_2Sr_{2.2}Ca_{0.8}Cu_2O_8$ crystals *Phys. Rev. Lett.* **60** 2194–7

[23] Wolff Fabris F, Mengotto Costa R, Fraga G L F, Pereira A S, Perottoni C A and Pureur P 2006 Splitting of the resistive transition in MgB_2 *Supercond. Sci. Technol.* **19** 405–9

[24] Janod E, Junod A, Graf T, Wang K Q, Triscone G and Muller J 1993 Split superconducting transitions in the specific heat and magnetic susceptibility of $YBa_2Cu_3O_x$ versus oxygen content *Physica* C **216** 129–39

[25] Menegotto Costa R, Jurelo A R, Rodrigues P Jr, Pureur P, Schaf J, Kunzler J V, Ghivelder L, Campá J A and Rasines I 1995 Splitting of the bulk resistive transition in high-T_c superconductors: evidence for unconventional pairing *Physica* C **251** 175–82

[26] Ghigo G, Botta D, Chiodini A, Gozzelino L, Gerbaldo R, Laviano F, Mezzetti E, Monticone E and Portesi C 2006 Effective gap at microwave frequencies in MgB_2 thin films with strong interband scattering *Phys. Rev.* B **71** 214522

[27] Rowell J M, Xu S Y, Zeng X H, Pogrebnyakov A V, Li Q, Xi X X, Redwing J M, Tian W and Pan X 2003 Critical current density and resistivity of MgB_2 films *Appl. Phys. Lett.* **83** 102–4

[28] Doi T, Masuda K, Fukuyama K, Hamada S, Kobayashi Yi, Hakuraku Y and Kitaguchi H 2007 Flux pinning centers in MgB_2 thin films prepared by an electron beam evaporation technique *IEEE Trans. Appl. Supercond.* **17** 2899–902

[29] Agassi D, Christen D K and Pennycook S J 2007 Thickness-dependent pinning in a superconductor thin film *J. Appl. Phys.* **101** 023916

[30] Herbstritt F, Kemen T, Marx A and Gross R 2002 Ultraviolet light assisted oxygenation process for submicron $YBa_2Cu_3O_{7-\delta}$ thin film devices *J. Appl. Phys.* **91** 5411–8
[31] Portesi C, Borini S, Taralli E, Rajteri M and Monticone E 2008 Superconducting MgB_2 nanobridges and meanders by electron beam lithography-based technique on different substrates *Supercond. Sci. Technol.* **21** 034006
[32] Carpinteri A 1994 Scaling laws and renormalization groups for strength and toughness of disordered materials. *Int. J. Solid Struct.* **31** 291–302